Clues to Variability in Arctic Minimum Sea Ice Extent

Jennifer A. Francis[1], Elias Hunter[1], Jeffrey R. Key[2], Xuanji Wang[3]
[1]Institute of Marine and Coastal Sciences, Rutgers University
[2]NOAA/NESDIS, Madison, WI
[3]CIMSS, University of Wisconsin-Madison

Accepted for publication in *Geophysical Research Letters*
22 September 2005

Corresponding author: Jennifer Francis, 74 Magruder Rd, Highlands NJ 07732
Tel: (732) 708-1217, Fax: (732) 872-1586, e-mail: francis@imcs.rutgers.edu

ABSTRACT

Perennial sea ice is a primary indicator of Arctic climate change. Since 1980 it has decreased in extent by about 15%. Analysis of new satellite-derived fields of winds, radiative forcing, and advected heat reveals distinct regional differences in the relative roles of these parameters in explaining variability in the northernmost ice edge position. In all six peripheral seas studied, downwelling longwave flux anomalies explain the most variability -- approximately 40% -- while northward wind anomalies are important in areas north of Siberia, particularly earlier in the melt season. Anomalies in insolation are negatively correlated with perennial ice retreat in all regions, suggesting that the effect of solar flux anomalies is overwhelmed by the longwave influence on ice edge position.

1. Introduction

The areal extent of Arctic sea ice has decreased dramatically in recent decades. While the decline is evident in all seasons since the 1970s, the summer trend of about 7.8 %/decade **(Fig. 1)** is approximately three times larger than the annual change [e.g., *Stroeve et al.,* 2005]. Regionally the changes vary substantially, both in magnitude and sign. In most of the peripheral seas, ice has decreased by 2 to 8%/decade, while the extent has increased north of the Canadian Archipelago and in the Bering Sea during winter [*Liu et al.,* 2004].

The causes of change in sea ice extent are expected to differ from region to region. Wind forcing is likely the primary driver in some areas, while thermodynamics will dominate in others. The apparent effect of large-scale atmospheric circulation patterns, such as the Northern Annular Mode/Arctic Oscillation and the El Niño Southern Oscillation, on observed sea ice change is described in *Liu et al.,* [2004]. While ice motions, horizontal heat transport, surface temperatures, and wind fields are clearly affected by trends in these patterns, they found only weak relationships with sea ice extent. *Kimura and Wakatsuchi* [2001] found that wind-driven ice motion explains much of the variation in *winter* ice extent in the Bering Sea, Barents Sea, and Sea of Okhotsk, but oceanographic forcing dominates in the Greenland and Labrador Seas. In this paper we expand these efforts to understand causes for variability in sea ice extent by investigating relationships between the perennial ice edge location and new satellite-derived dynamic and thermodynamic forcing parameters. These include downwelling longwave and shortwave radiation fluxes, zonal and meridional winds, and advective heating in six Arctic peripheral seas over the 26-year period from 1979 to 2004.

2. Data and Methodology

Sea ice concentrations based on a modified version of the NASA Bootstrap Algorithm were obtained from the National Snow and Ice Data Center (NSIDC) [*Comiso*, 2002]. Beginning with daily values from 1979 to 2004, the ice edge was located in six peripheral seas: Barents, Kara, Laptev, E. Siberian, Chukchi, and Beaufort. In each region, the edge was identified as the southernmost location of 50% concentration along three longitude lines separated by two degrees and centered on those listed in **Table 1.** These were selected as being central to each sea and likely representative of the ice behavior in that area. The distance from the mean position of these three points directly southward to the coast was recorded as a time series, except in the Barents Sea, where an arbitrary reference point was used for convenience. After applying a 10-day smoother, the location and date of the maximum distance of the ice edge from the coast in each sea was identified as the annual-maximum ice retreat. The 26-year mean maximum distance was subtracted to obtain the annual-maximum ice retreat anomalies (hereafter **MIAs**), shown in **Fig. 2**.

Time series for each of the following parameters were generated by subsetting daily-mean, gridded, satellite-derived fields in an area within 400 km of the positions listed in **Table 1**, which are the approximate mean northernmost positions of the ice edge along selected longitudes in each sea. Anomalies for each parameter were then calculated from the time series for each region by dividing and averaging the series into 10-day means. A 26-year mean for each 10-day interval was then subtracted from individual averages to obtain anomalies, which were normalized by the standard deviation. Time series of normalized anomalies were correlated with MIA using a standard multiple regression technique. Variances in MIA explained by each variable (expressed as the squared partial correlation coefficient) were calculated for lags from 0 to 90 days (MIAs lag forcings) in each region.

Surface downwelling longwave fluxes **(DLFs)** over the Arctic were calculated using products derived from the TIROS Operational Vertical Sounder (TOVS) according to the basic method explained in *Francis* [1997], but with many recent improvements. Daily DLF fields were produced over the region north of 60°N at a $(100\ km)^2$ spatial resolution from June 1979 through 2004. Eight years of measurements from the Surface Heat Budget of the Arctic (SHEBA) experiment in the Beaufort Sea (Oct. 1997 to Oct. 1998) and from the Atmospheric Radiation Measurement Program's site at Barrow, Alaska (1998-2004) were used for validation. The bias, standard error, and correlation of daily mean values are approximately 11 W m^{-2}, 30 W m^{-2}, and 0.7 respectively. The 10-day filter applied to radiative flux retrievals reduces the errors substantially.

Downwelling shortwave radiation fluxes **(DSFs)** from the extended Advanced Very High Resolution Radiometer (AVHRR) Polar Pathfinder (APP-x) project were only available for the period 1982 to 2000 [*Key*, 2002; *Wang and Key*, 2005]. Flux retrievals wee provided at a 25-km spatial resolution, and have been validated with measurements from the SHEBA field experiment. The bias and root-mean-square error are approximately 10 and 34 W m^{-2}. Inter-satellite calibration errors are negligible over the AVHRR data record [*Wang and Key*, 2003]. Surface albedo was not used in this analysis for two reasons: 1) sea ice extent within our 400-km-radius subsets are obviously strongly correlated with albedo, and 2) the APP-x albedos appeared to be unrealistically low during the melt season.

Three-dimensional Arctic winds were derived from TOVS temperature profiles following the method described in *Francis et al.,* [2005]. The TOVS winds exhibit significantly smaller biases than do reanalysis winds as compared to independent rawinsonde measurements [*Francis et al.,* 2005]. For this application, poleward **(V)** and zonal **(U)** winds averaged from 10 m to 850 hPa are used to represent the large-scale, lower-tropospheric circulation.

The horizontal convergence of sensible heat, expressed as a daily mean heating rate, was calculated from temperature profiles and upper-level wind fields, both retrieved from TOVS. The heating averaged in the 1000-to-850 hPa layer **(ADV)** is used in this analysis. Additional details can be found in *Francis* [1994].

3. Results

Figure 2 presents time series of anomalies (relative to the 1979-to-2004 mean) in the maximum ice edge retreat along selected longitude bands in regions defined in **Table 1**. While interannual variability is large, trends are statistically significant (> 90%) in the Pacific-sector seas: E. Siberian, Chukchi, and Beaufort. Time series for the E. Siberian and Laptev Seas are significantly correlated (> 90%) with the winter North Atlantic Oscillation index, consistent with the findings of *Rigor and Wallace* [2004].

Figure 3 displays variances in MIAs in each region explained by the forcing parameters. Histogram bars represent the total explained variance at lags of 0, 10, 25, 50, and 80 days prior to the date of maximum ice retreat in each sea. The colored segments represent the fractional amount of variance explained by each of the forcing parameters. Correlations between DSF anomalies and MIAs are negative in all six seas (**Table 2**), implying that *DSF anomalies do not drive perennial ice-edge variability.* This conclusion is supported by strong negative lagged correlations between DSF and MIAs, with ice retreat leading the DSF anomaly. This behavior could result from two effects. As sea ice retreats, the area-average albedo decreases, multiple reflections of shortwave radiation between clouds and the surface decrease, which reduces the DSF. Increased open water may also provide additional moisture for cloud formation, further reducing DSF. This result is consistent with observed increasing trends in spring cloud cover over the Arctic Ocean since 1979

[*Wang and Key,* 2003, 2005; *Schweiger*, 2004]. While reduced sea ice will allow additional solar radiation to be absorbed by the ocean, contributing to further melt, the *anomalies* in DSF do not appear to drive perennial ice edge anomalies; in fact, they may constitute a negative feedback on the system. Consequently, DSF anomalies are excluded from the multiple regression analysis presented in **Fig. 3** and from the following discussion.

The most striking feature of **Fig. 3** is the prevalence of green in the histogram bars, indicating the high degree of variance in MIAs explained by DLF anomalies. Correlations between MIAs and DLF anomalies are uniformly positive in all areas, i.e., positive anomalies in DLF correspond to less perennial ice. Surprisingly, wind anomalies (blue, black) and advective heating (red) have a relatively weak influence overall. The following discussion begins in the Barents Sea and progresses eastward around the Arctic Ocean.

In the **Barents Sea**, DLF is by far the strongest influence on MIAs during the month preceding maximum ice retreat, while in spring easterly (from the east) winds and advective heating also play a role. Over half of the MIA variance is unexplained by these four parameters; we expect ocean influences are important in this region.

Advective heating explains nearly as much variance in MIA as does DLF at a zero lag in the **Kara Sea**. In the Kara and adjacent **Laptev Sea**, the MIAs appear to be most strongly influenced by forcing anomalies near the time of maximum retreat. It appears, however, that southerly wind anomalies in both of these seas explain nearly as much ice-edge variance as does DLF, particularly early in the melt season. The wind-driven advection of ice away from the coast likely enhances the effect of thermodynamic anomalies, as suggested by *Rigor et al.* [2002].

In the **E. Siberian Sea** the DLF anomalies again explain most of the variance, particularly during the month prior to maximum ice retreat. As was the case in the nearby Laptev Sea, southerly wind anomalies at the time of maximum ice retreat are also influential. Less than half of the total MIA variance can be explained by these four forcing parameters, suggesting that other factors (e.g., river discharge, snow depth, and/or ocean currents) are also important.

Variance in MIAs in the **Chukchi Sea** are explained primarily by DLF at all lags, advective heating during the month prior to maximum retreat, and meridional winds early in the melt season. In contrast to the E. Siberian Sea, over half of the variance in MIAs is explained by anomalies in the four forcing parameters.

Finally in the **Beaufort Sea,** the MIA variance appears to be dominated by DLF, but anomalies several weeks prior to the maximum ice retreat have the largest influence. This pattern appears consistent with the recent thinning of ice in this area and consequent susceptibility to thermodynamic forcing suggested by *Rigor and Wallace* [2004].

4. Discussion and Conclusions

New satellite-derived atmospheric parameters are used to quantitatively assess relationships between variability in maximum sea ice retreat and five factors that are expected to drive it: zonal and meridional winds, sensible heat advection, and downwelling fluxes of longwave and shortwave radiation. Each of six peripheral seas -- Barents, Kara, Laptev, E. Siberian, Chukchi, and Beaufort -- exhibits distinct characteristics as to the relative importance of these factors in explaining anomalies in MIAs. While explained variance does not necessarily imply a cause-and-effect relationship, this analysis suggests that downwelling longwave radiation fluxes account for a large percentage -- approximately 40% on average -- of the variability in perennial

ice extent from 1979 to 2004. In the Beaufort/Chukchi Sea area, increasing ice retreat is consistent with strong positive trends in spring DLF, which appear to be caused by substantial increases in precipitable water, cloud amount, and surface temperature (not shown). Not only do DLF anomalies explain the most variance in MIAs, they compensate for anticorrelated anomalies in insolation. Indeed, as is the case for the interactions between MIAs and solar fluxes, the relationship between DLF and ice edge position is also two-way. Additional open water will likely be warmer than the ice it replaced, and thus be a stronger emitter of longwave radiation. Cloud bases would absorb this energy, warm, and emit more radiation toward the surface. This relationship is a positive feedback in the system.

Anomalies in meridional winds also explain significant variance in most areas except for the Barents and Beaufort Seas, but the influence is much weaker than expected. Links between ice extent and the NAO have been suggested by many investigators, but it appears that the primary effects are through thermodynamics rather than direct mechanical wind forcing. There is evidence, however, that the relative roles of dynamics and thermodynamics may be evolving. An earlier analysis for the 1979-to-2001 period revealed a stronger dynamical influence, particularly in Pacific areas [*Francis et al.,* 2005].

Counter-intuitively, anomalies in the downwelling shortwave flux are negatively correlated with ice retreat anomalies in all seas and at all lags, i.e., positive (negative) DSF anomalies are associated with more (less) ice. This suggests that DSF anomalies act as a negative feedback on the system and do not explain variability in the position of the perennial ice edge. Other factors not considered in this study likely contribute to the variance in MIAs, including ice surface albedo, snowpack depth, river discharge, and ocean circulation. These variables will be investigated to the extent possible in future studies.

The Arctic climate system appears to be marching steadily toward a new state, as permanent ice in all its forms is diminishing rapidly. Some of the most reliable and disturbing evidence is the loss of perennial sea ice, which in the past three summers (2002-2004) has set new records for minimum extent [*e.g., Stroeve et al.,* 2005]. The results of this study provide quantitative evidence for the varying roles of dynamics and thermodynamics in explaining these dramatic changes. A redistribution of ice thickness owing to changes in the atmospheric circulation [*Rigor and Wallace*, 2004] may have set the stage for DLF-driven ice loss in recent years. The looming question now is whether enough sea ice has melted to trigger the model-predicted ice-albedo feedback, as suggested by *Serreze and Francis* [2005] and *Lindsay and Zhang* [2005]. Clearly, an understanding of the causes and future trajectory of the Arctic system is imperative for advancing climate science, for evaluating and interpreting model simulations, and for predicting impacts on ecological systems and society.

Acknowledgements This work was supported by grants from NASA (NAGW-2407, NAG5-4908), NSF (OPP-0105461 and 0240791), and the DOE/ARM program (DE-FG02-02ER63313). We are grateful to Ms. Jaclyn Secora for programming assistance and to Drs. J. Miller, A. Broccoli, R. Stone, and D. Douglas as well as the two anonymous reviewers for helpful suggestions.

5. References

Comiso, J.C. (2002), Bootstrap sea ice concentrations for NIMBUS-7 SMMR and DMSP SSM/I, June to Sept. 2001. Boulder, CO, USA: National Snow and Ice Data Center. Digital media.

Francis, J.A., E. Hunter, and C.-Z. Zou (2005), Arctic tropospheric winds derived from TOVS sat-

ellite retrievals. *J. Clim., 18*, 2270-2285.

Francis, J.A., E. Hunter, J.R. Key, and X. Wang, (2005), Attribution of variability in Arctic minimum sea ice extent, paper presented at 8th Conference on Polar Meteor. and Oceanog., Amer. Meteor. Soc., San Diego, Calif.

Francis, J.A. (1997), A method to derive longwave fluxes at the Arctic surface from TIROS operational vertical sounder data, *J. Geophys. Res., 102,* 1795-1806.

Francis, J.A. (1994), Improvements to TOVS retrievals over sea ice and applications to estimating Arctic energy fluxes, *J. Geophys. Res., 99,* 10,395-10,408.

Key, J. (2002), The Cloud and Surface Parameter Retrieval (CASPR) System for Polar AVHRR User s Guide, Cooperative Institute for Meteorological Satellite Studies, University of Wisconsin, 1225 West Dayton St., Madison, WI 53562, 61 pp.

Kimura, N. and M. Wakatsuchi (2001), Mechanisms for the variation of sea-ice extent in the Northern Hemisphere, *J. Geophys. Res., 106 (C12),* 31319-31332.

Lindsay, R. W., and J. Zhang (2005), The thinning of arctic sea ice, 1988-2003: Have we reached the tipping point?, paper presented at 8th Conference on Polar Meteor. and Oceanog., Amer. Meteor. Soc., San Diego, Calif.

Liu, J., J.A. Curry, and Y. Hu (2004), Recent Arctic sea ice variability: connections to the Arctic oscillation and the ENSO. *Geophys. Res. Lett., 31,* doi:10.1029/2004GL019858.

Rigor, I.G., J.M. Wallace, and R.L. Colony (2002), Response of sea-ice to the Arctic Oscillation, *J. Clim., 15,* 2648-2663.

Rigor, I.G. and J.M. Wallace (2004), Variations in the age of Arctic sea-ice and summer sea-ice extent, *Geophys. Res. Lett., 31,* L09401, doi:10.1029/2004GL019492.

Schweiger, A.J. (2004), Changes in seasonal cloud cover over the Arctic seas from satellite and

surface observations. *Geophys. Res. Lett., 31*, doi:10.1029/2004GL020067.

Serreze, M.C. and J.A. Francis (2005), The Arctic amplification debate. *Clim. Change*, in press.

Stroeve, J.C., M.C. Serreze, F. Fetterer, T. Arbetter, W. Meier, J. Maslanik, and K. Knowles (2005), Tracking the Arctic's shrinking ice cover: another extreme minimum in 2004. *Geophys. Res. Lett., 32,* L04501, doi:10.1029/2004GL021810.

Wang, X. and J.R. Key (2003), Recent trends in Arctic surface, cloud, and radiation properties from space. *Science, 299,* 1725-1728.

Wang, X. and J.R. Key (2005), Arctic surface, cloud, and radiation properties based on the AVHRR Polar Pathfinder dataset. Part I: spatial and temporal characteristics. *J. Clim,* in press.

6. Tables

Table 1: Selected locations in peripheral seas

Region	Latitude	Longitude [deg. E]
Barents Sea (BA)	78	30
Kara Sea (KA)	79	80
Laptev Sea (LA)	76	120
E. Siberian Sea (ES)	75	160
Chukchi Sea (CH)	73	190
Beaufort Sea (BE)	71	220

Table 2: Sign of correlation (>90% confidence) between anomalies in maximum ice retreat and anomalies in forcing parameters from 1979 to 2004. Varying sign at different lag values is indicated by +/- . Non-significant correlations are indicated by n/s. DSF correlations are calculated for 1982 to 2000 only.

Region	u	v	DLF	DSF	ADV
Barents Sea	+/-	+	+	–	+/-
Kara Sea	–	+	+	–	+
Laptev Sea	n/s	+	+	–	+/-
E. Siberian Sea	+	+	+	–	+
Chukchi Sea	+	+	+	–	+
Beaufort Sea	+/–	n/s	+	–	+

7. Figures

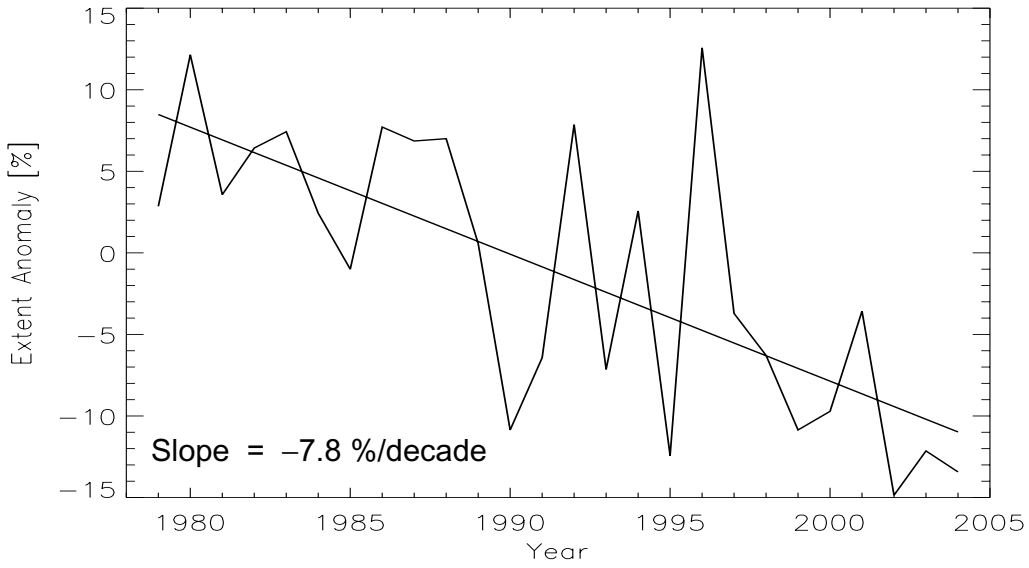

Figure 1: Anomalies in September-average total sea ice extent (area with >15% concentration) in the N. Hemisphere derived from passive microwave satellite data. Anomalies are relative to the 1979-2000 mean of 7.0 million km^2. Data were obtained from the National Snow and Ice Data Center.

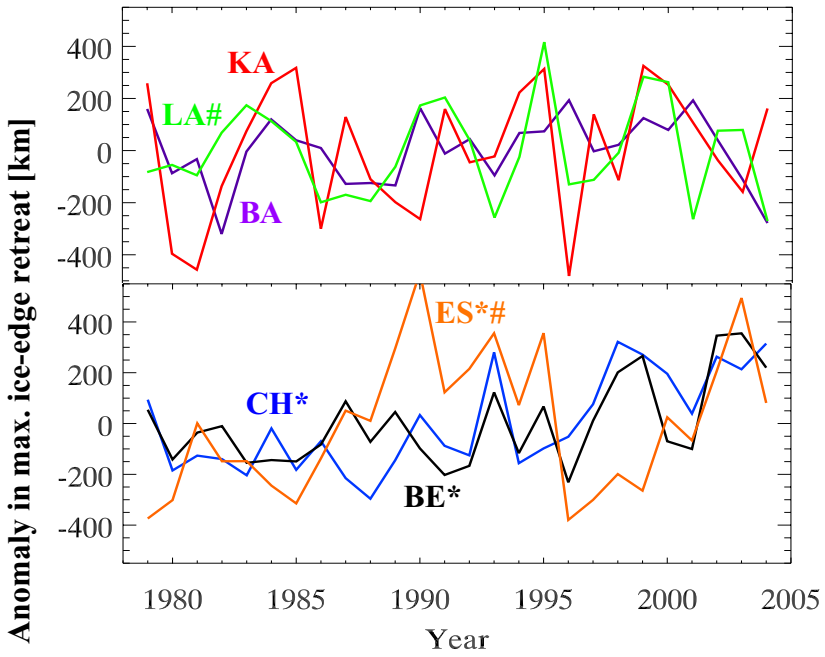

Figure 2: Time series of anomalies in maximum ice-edge retreat along selected longitudes denoted by two-letter abbreviations defined in Table 1. The ice edge is defined by the southernmost 50% ice concentration in retrievals from passive microwave satellite data. A * indicates a statistically significant (>90% confidence) trend, # denotes significant correlation with the winter NAO index.

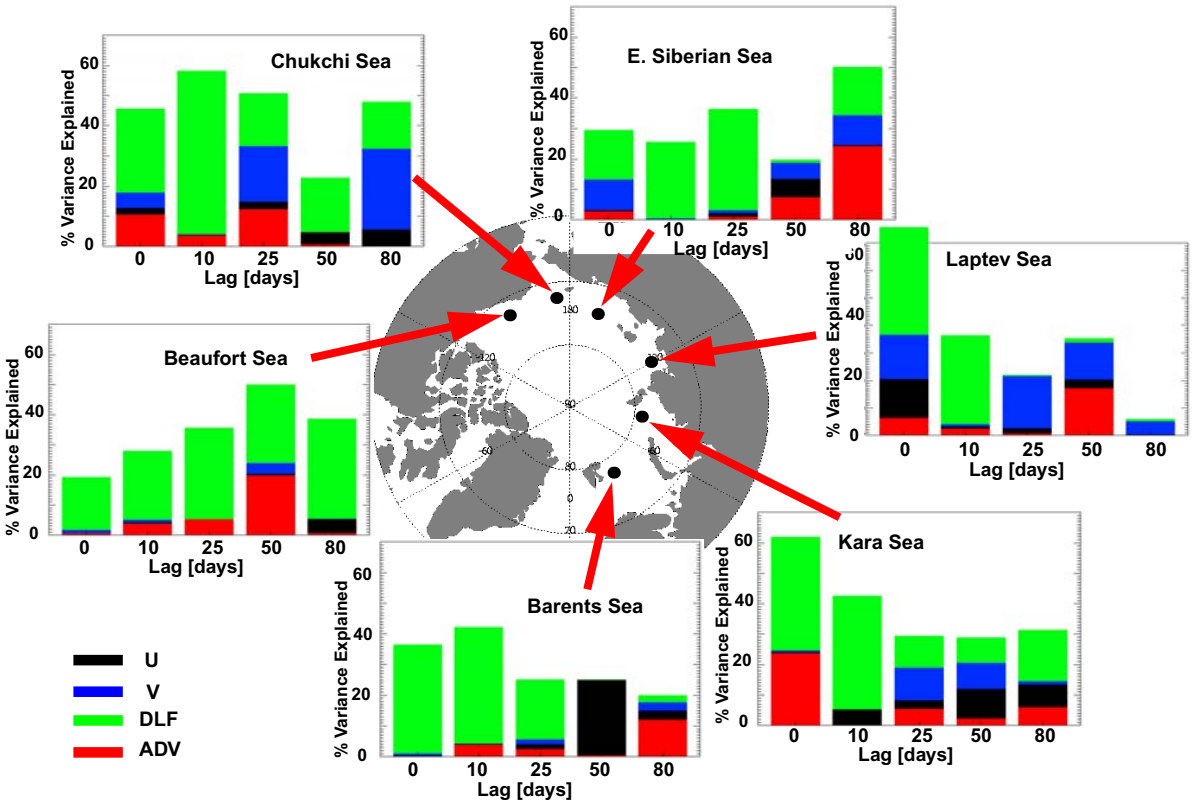

Figure 3: Percentages of variance (y-axis) in anomalies of sea ice maximum retreat explained by anomalies in zonal wind (U, black), meridional wind (V, blue), downwelling longwave flux (DLF, green), and the convergence of advected sensible heat (ADV, red) in each peripheral sea of the Arctic Ocean. The bars represent explained variance at lags of 0, 10, 25, 50, and 80 days, where the ice edge anomaly lags the forcing anomaly. Black dots mark locations in Table 1.